Chapter 5

Collectivity, Transfer and Fusion Enhancement

5.1 The Systems ^{40}Ca + ^{90,96}Zr as a Test-Case

As described in Chapter 1, the dominant internal degrees of freedom of the nuclear binary system are collective excitations of the reactants and nucleon transfer reactions between them. For light systems ($Z_pZ_t \lesssim 1500$) collective rotational and vibrational excitations are often seen to have larger effects on the reaction dynamics than transfer reactions. For example the coupling schemes for ^{16,17}O + ^{144}Sm have been found[1] to be dominated by the lowest energy octupole state in ^{144}Sm. The positive Q-value one-neutron stripping channel in ^{17}O + ^{144}Sm, which is the strongest transfer reaction in this system, results only in a minor modification of the barrier distribution. Similarly[2], for ^{58}Ni + ^{60}Ni contrary to expectation the reaction dynamics are not much affected by the zero Q-value two-neutron transfer channel, but are dominated by single and double phonon excitations of the lowest energy quadrupole states in ^{58}Ni and ^{60}Ni. This dominance of a few strongly coupled states in lighter systems enables a successful description of the reaction within the truncation limit of the generalized barrier problem using the coupled-channels model, which is a 'microscopic' model.

For heavier systems ($Z_pZ_t \gtrsim 1500$) a 'macroscopic' model has been invoked, which is based on transport theory, as described in Section 1.5.5. The choice of this model can be justified because of the apparent energy dissipation preceding the fusion of these systems, which has its manifestation in the observed 'extra-push' energy. The occurence of dissipation indicates the presence of a large number of weakly coupled internal degrees of freedom. Whereas the number of vibrational and rotational degrees of freedom does not change significantly with increasing Z_pZ_t, the number of possible nucleon transfer reactions rises dramatically because of the larger overlap during the collision. In the extreme limit, fusion between very heavy nuclei may thus be depicted as the result of the nucleon (mainly neutron) flow between the two reactants. This enables a 'macroscopic' treatment with transport theory, which explains the extra-push phenomenon, as shown in Figure 1.14. The same arguments justify the application of the more schematic models of neck-formation[3–6].

[1] J.R. Leigh *et al.*, Phys. Rev. C **52** (1995) 3151.

[2] A.M. Stefanini *et al.*, Phys. Rev. Lett. **74** (1995) 864.

[3] U. Jahnke *et al.*, Phys. Rev. Lett. **48** (1982) 17.

[4] H.J. Krappe *et al.*, Z. Phys. A **314** (1983) 23.

[5] A. Iwamoto, K. Harada, Z. Phys. A **326** (1987) 201.

[6] J. Schneider, H.H. Wolter, Z.Phys. A **339** (1991) 177.

The question arises if and where there is a transition between the two limits of the generalized barrier problem as represented by 'microscopic' channel-coupling and 'macroscopic' neck-formation. It may be expected that the two approaches are complementary for some systems. In addition one may ask, if there are signatures of dissipation in lighter systems and/or if states which strongly couple in lighter systems, like the octupole vibrational states, also affect heavy systems despite the dominance of the mass-flow.

As pointed out in Section 1.5.4, it has been suggested[7] that the flow of neutrons between the reactants may initiate fusion already at large inter-nuclear separations. This effect, if it occurs, may constitute the suspected transition between channel-coupling and mass-flow. Neutron-flow is expected to correspond to a flat barrier distribution with the left edge of the distribution being the lowest energy for which the distance of closest approach allows neutrons to transfer between the two potential wells. If such flat barrier distributions exist, it should be possible to identify them through precision measurements of their experimental representations $D^{fus,qel,el}(E)$ which have been discussed in the previous chapters.

The comparison of the two reactions ^{40}Ca + ^{90,96}Zr should be particularly well suited to isolate the effects of neutron-flow. The projectile ^{40}Ca is a closed shell nucleus, so that its influence on the fusion process may be negligible. This expectation is confirmed by the results for the fusion of ^{40}Ca + ^{40}Ca displayed in Figure 1.13, which show no coupling effects. Thus the fusion dynamics should be dominated by the properties of the two target nuclei. Among the even-even Zirconium isotopes, ^{96}Zr is the one which is most like the neutron magic ^{90}Zr. This is illustrated in Figure 1.3. Both isotopes are spherical with similar shell structures. In both cases the lowest quadrupole and octupole states are moderately collective and may be expected to play a similar role in the fusion dynamics. The two reactions differ, however, distinctively in their neutron transfer Q-values, as is illustrated in Table 3.2. In the heavier system up to 8 neutrons can be transferred with positive Q-values from ^{96}Zr to ^{40}Ca making this reaction a good candidate for neutron-flow. In contrast, the Q-values for the respective channels in the lighter system are all negative, which should suppress the effect.

Since the detection of elastic scattering in ^{40}Ca + ^{96}Zr is difficult because of the many positive Q-value transfer channels, the distribution $D^{el}(E)$ is not easily determined for this reaction. Thus precision measurements of the distributions

[7]P.H. Stelson, Phys. Lett. B **205** (1988) 190.

$D^{fus}(E)$ and $D^{qel}(E)$ are best suited to extract the barrier structures of the two reactions. The discussion of these distributions as measured for ^{40}Ca + ^{90,96}Zr, which was commenced in Section 3.5, is continued in this chapter, which also gives an account of the experimental details.

5.2 Experimental Details

The experiments to study the reactions ^{40}Ca + ^{90,96}Zr were performed at the XTU tandem accelerator facility of the Legnaro Laboratories. The targets were 50 μg/cm^2 of isotopically enriched zirconium which was evaporated on 15 μg/cm^2 carbon foils.

The beam energy E_{lab} was defined with an uncertainty of less than 100 keV by a 90° analysing magnet. In order to measure the fusion cross sections well above and below the Coulomb barrier which is at about 140 MeV for both systems, E_{lab} was varied between 125 and 160 MeV. To optimize the accuracy of the beam energy it was only changed downwards in 0.5 MeV and 1 MeV steps starting at 160 MeV. For each energy the beam was focused to the same position in the target plane using a fluorescent quartz.

The ^{40}Ca projectiles were in the 10^+ charge state and the beam current was typically 100 nA. The beam intensity was monitored continuously by four silicon surface barrier detectors which detected Rutherford scattering from the target. The detectors were located on the corners of a square in a plane perpendicular to the beam and at scattering angles of $\theta_{lab} = 22°$ relative to the beam direction. Variations of the four monitor count rates during the experiments were assumed to be caused by slight changes in the beam direction due to different beam focusing. Using an optimization routine these variations have been corrected for. The evaporation residues at $\theta_{lab} = 0°$ were separated from most of the intense flux of beam-like particles using an electrostatic deflector and detected by measuring the time-of-flight and residual energy as described in Chapter 2.

At $E_{lab} = 152$ MeV and 140 MeV the angular distribution of the evaporation residue yield was measured for both systems. The detection angle was varied in 1° steps between $\theta_{lab} = 0°$ and $-7°$. In addition, the yield was measured at $\theta_{lab} = +2°$ and $+4°$. The four angular distributions are symmetric about 0°. For each system the angular distribution at $E_{lab} = 152$ MeV agrees within experimental uncertainties with the distribution at 140 MeV, so that the two distributions have been combined.

These combined angular distributions are shown in Figure 5.1(b) for both sys-

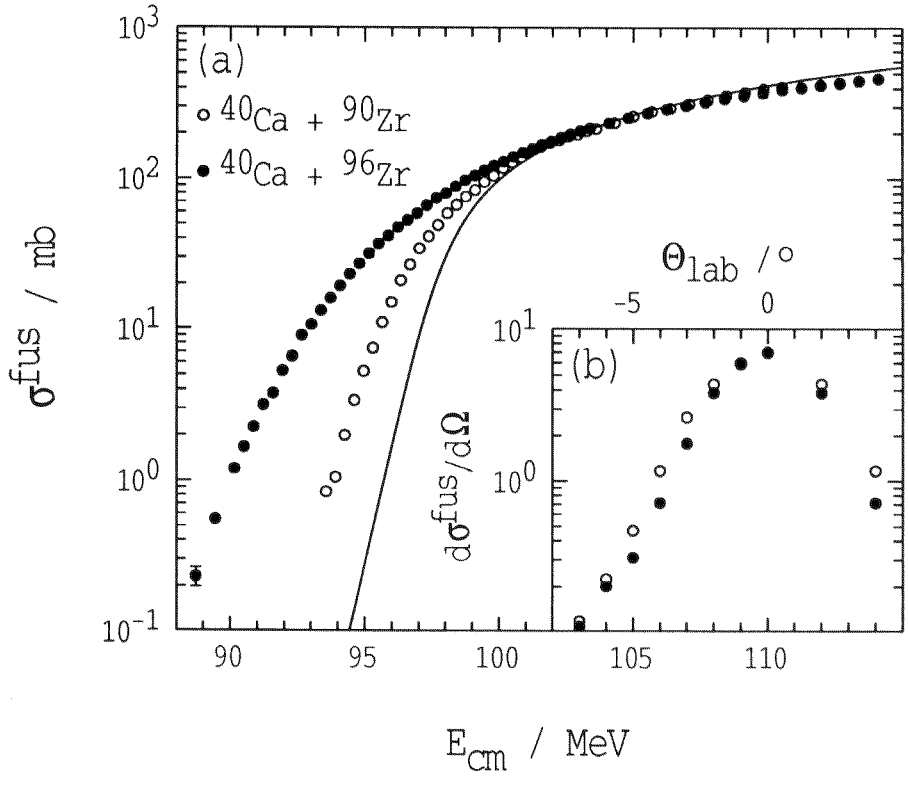

Figure 5.1: *(a) The fusion excitation functions for ^{40}Ca + $^{90,96}Zr$. The statistical uncertainties of the cross sections are smaller than the symbol size. The fusion excitation function for ^{40}Ca + ^{96}Zr has been normalized to the one for ^{40}Ca + ^{90}Zr. The solid curve is a single barrier calculation. (b) The fusion angular distributions for the two systems in arbitrary units. The results for E_{lab} = 140 MeV and 152 MeV have been combined. The horizontal axis is labelled above the panel.*

tems. In contrast to the lighter system, the distribution for ^{40}Ca + ^{96}Zr shows the onset of a shoulder at large angles. This is presumably due to an increase in α-particle emission. nucleus. At angles more backward than $-7°$ the evaporation residue yield has been extrapolated. By integrating the angular distributions the ratio R_{tot} of the yield at $\theta_{lab} = 0°$ relative to the total yield of evaporation residues has been obtained for both systems. The solid angles of the monitor detectors were measured after the experiments using an α-source located at the beam position in the target plane. The four values obtained are closely distributed around 0.92×10^{-4} sr.

For each energy the number of evaporation residue events has been normalized to the Rutherford scattering detected by the monitor detectors. Using the measured solid angles, the 0°-to-total ratio R_{tot} and the transmission factor, these evaporation

residue yields have been transformed into total cross sections. Since fission of the compound nucleus can be neglected for both systems, the measured cross sections have been taken as fusion cross sections σ^{fus}. They are given in the Appendix in Table A.9 and plotted in Figure 5.1(a). The energies have been corrected for losses in the target foil. The statistical uncertainties of the cross sections are of the order of 1%. The systematic accuracy of the excitation functions is 7%, with the transmission of the electrostatic deflector being the major source of uncertainty.

In order to remove differences due to the different sizes of the target nuclei, the excitation function for ^{40}Ca + ^{96}Zr in Figure 5.1(a) has been normalized to the one for ^{40}Ca + ^{90}Zr by multiplying the energies with the ratio of the average barriers B_0 of the two systems, which is 1.013, and by multiplying the cross sections with the square of the ratio of their average fusion radii R_0, which is 0.971. This normalization of the data for ^{40}Ca + ^{96}Zr is maintained throughout this chapter.

5.3 Discussion of the Experimental Data

The experimental fusion cross sections in Figure 5.1(a) show at low energies an enhancement relative to a one-dimensional barrier penetration calculation shown as solid curve. Whereas the two experimental excitation functions agree above E_{cm} = 105 MeV, they differ at the lowest energies by more than an order of magnitude. The enhancement and the isotopic variations in the magnitude of the enhancement may be thought to be caused by the presence of a distribution of potential barriers rather than a single barrier, as has been shown in Section 1.5. Representations $D^{fus}(E)$ of this barrier distribution can be extracted from the measured fusion excitation function using the point-difference formula given in Equation 1.60.

For the two excitation functions in Figure 5.1(a) the energy step width ΔE_{cm} in Equation 1.60 has been varied between 0.35 and 5 MeV. This resulted in 14 representations of the barrier distribution for each system. In Figure 5.2 it is illustrated how a gradual loss of sensitivity to the barrier structure is accompanied by an improvement of experimental precision of $D^{fus}(E)$ as ΔE_{cm} is increased. For both systems the various representations of the barrier distribution are consistent with each other.

In the case of ^{40}Ca + ^{90}Zr two peaks are resolved at E_{cm} = 96 MeV and 99 MeV. The representations of $D^{fus}(E)$ with $\Delta E_{cm} \geq 2.1$ MeV which are well defined at high energies show in addition a small peak at 103.5 MeV. The distribution as a

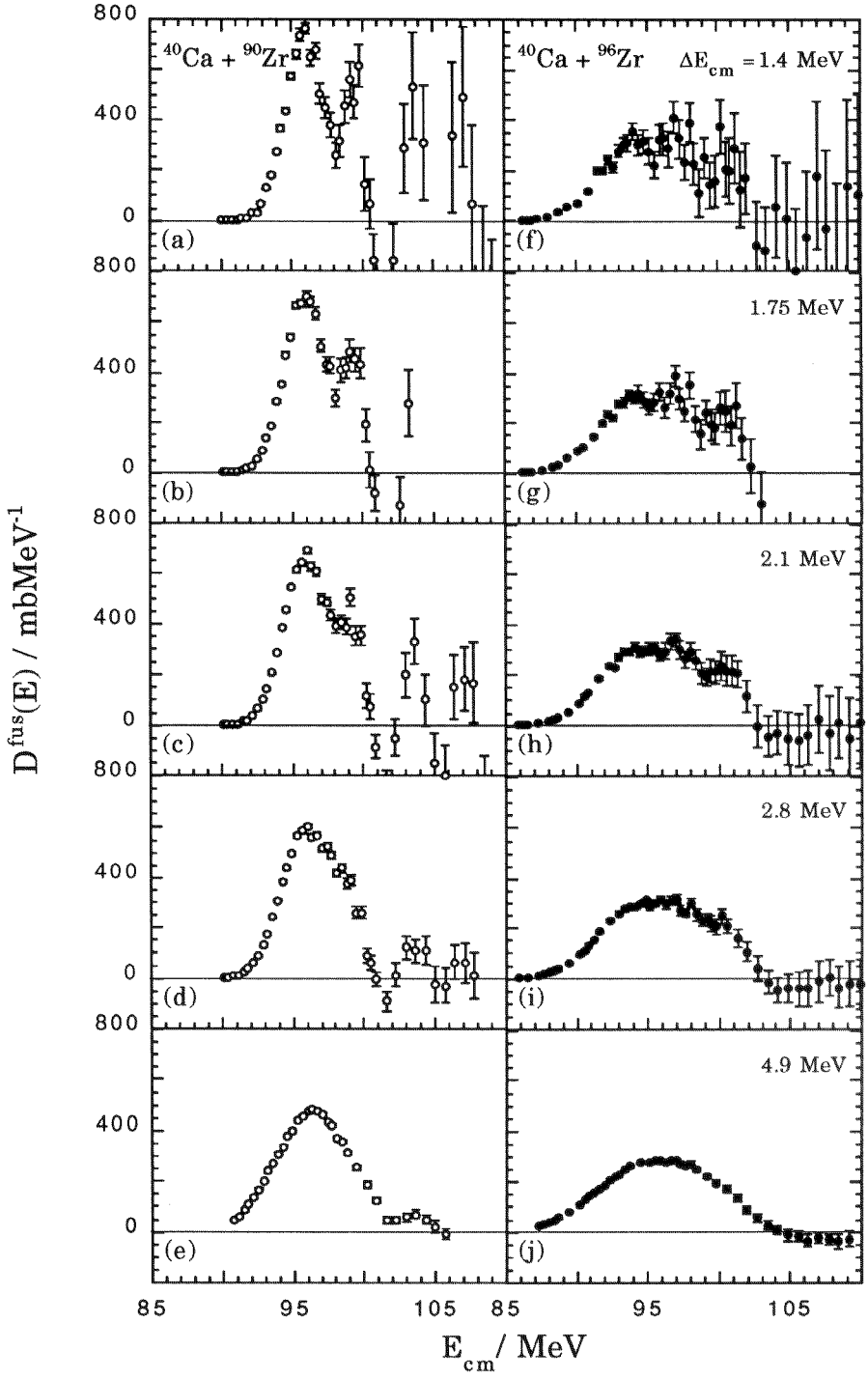

Figure 5.2: *Representations $D^{fus}(E)$ of the barrier distributions for $^{40}Ca + ^{90}Zr$ (a–e) and $^{40}Ca + ^{96}Zr$ (f–j). The representations have been extracted from the fusion excitation functions. The energy steps ΔE_{cm} used in the point-difference differentiation are given in the figure for adjacent panels.*

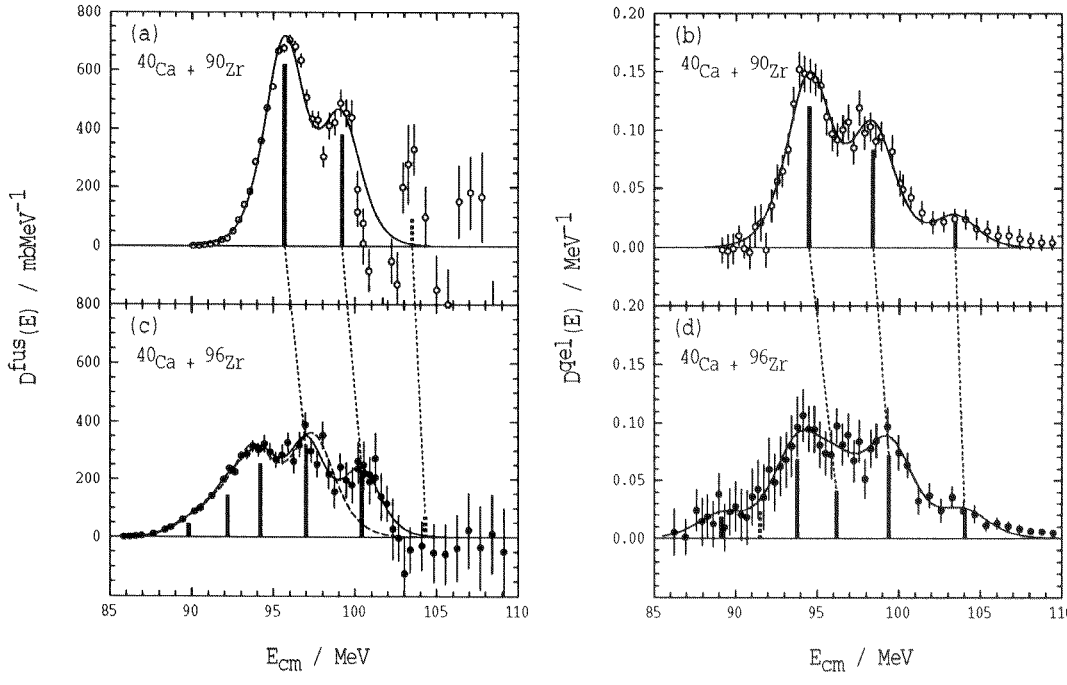

Figure 5.3: *Systematic analysis of the experimental barrier distribution representations $D^{fus,qel}(E)$ within the eigen-channel model as discussed earlier. The best fits to the data are shown as solid curves. The long-dashed curve in panel (c) is a three barrier fit. The extracted fusion barriers are indicated as solid bars. Dashed bars are tentative.*

whole is much narrower and taller than in the case of ^{40}Ca + ^{96}Zr. For this latter system $D^{fus}(E)$ is rather flat and wide. Peaks may be identified at E_{cm} = 94 MeV, 97 MeV and 101 MeV.

In parallel with the fusion excitation functions quasi-elastic scattering at θ_{cm} = 136° has been measured for both systems. This part of the experiment and the extraction of the barrier distribution representations $D^{qel}(E)$ have been described in Section 3.5, where the two complementary representations $D^{fus}(E)$ and $D^{qel}(E)$ have also been analysed empirically within the eigen-channel model. For convenience the results of this analysis are displayed here again in Figure 5.3. A comparison of the barrier structures of the two systems shows that above 95 MeV both systems have three barriers with very similar heights and weights. Below 95 MeV no other barriers are present in the reaction ^{40}Ca + ^{90}Zr, whereas for ^{40}Ca + ^{96}Zr at least three additional barriers exist. This marks an important difference between the two systems.

5.4 Comparison with the Neutron-Flow Model

The experimental distributions $D^{fus,qel}(E)$ for $^{40}Ca + ^{96}Zr$ are reminiscent of the rectangular ones suggested[8,9] by Stelson. Adopting a concept discussed earlier[10], Stelson proposed that fusion may be initiated at large distances, when it is possible for neutrons to flow between the colliding nuclei. The largest distance for which neutron-flow can occur corresponds to a threshold barrier which marks the low energy edge of the rectangular distribution. Thus broad distributions would correspond to neutron-flow over large distances. Exploring these ideas, the parametrisations of the barrier distributions for $^{40}Ca + ^{90,96}Zr$ suggested by the neutron-flow model and differentiated in the same way as the data are compared with the measured $D^{fus}(E)$ in Figure 5.4 whereby quantum tunnelling has been taken into account. For both systems the Stelson-parametrisations are first order approximations of the experimental distributions. For $^{40}Ca + ^{96}Zr$, the parametrisation, using a mean barrier $B_m = 96.4$ MeV and a threshold barrier $B_t = 91.2$ MeV, has the flat and broad shape associated with neutron-flow. The question arises as to whether the physical neutron transfer couplings in $^{40}Ca + ^{96}Zr$ can reproduce this shape.

5.5 Coupled-Channels Calculations

In order to understand the coupling schemes which give rise to the barrier structures extracted from the experimental data and shown in Figure 5.3, simplified and exact coupled-channels calculations have been carried out. They are discussed in the following sections.

5.5.1 Nuclear Structure Considerations

The double shell closure at $Z, N = 20$ makes the nucleus ^{40}Ca a relatively inert projectile. It has been found that the fusion excitation function for the reaction $^{40}Ca + ^{40}Ca$ shows no sub-barrier enhancement[11]. It may therefore be expected that the internal properties of ^{40}Ca play a negligible role in the fusion of this nucleus with $^{90,96}Zr$. Nevertheless possible effects of projectile excitation have been studied

[8] P.H. Stelson, Phys. Lett. B **205** (1988) 190.

[9] P.H. Stelson *et al.*, Phys. Rev. C **41** (1990) 1584.

[10] W. von Oertzen *et al.*, Z. Phys. A **326** (1987) 463.

[11] H.A. Aljuwair, Phys. Rev. C **30** (1984) 1223.

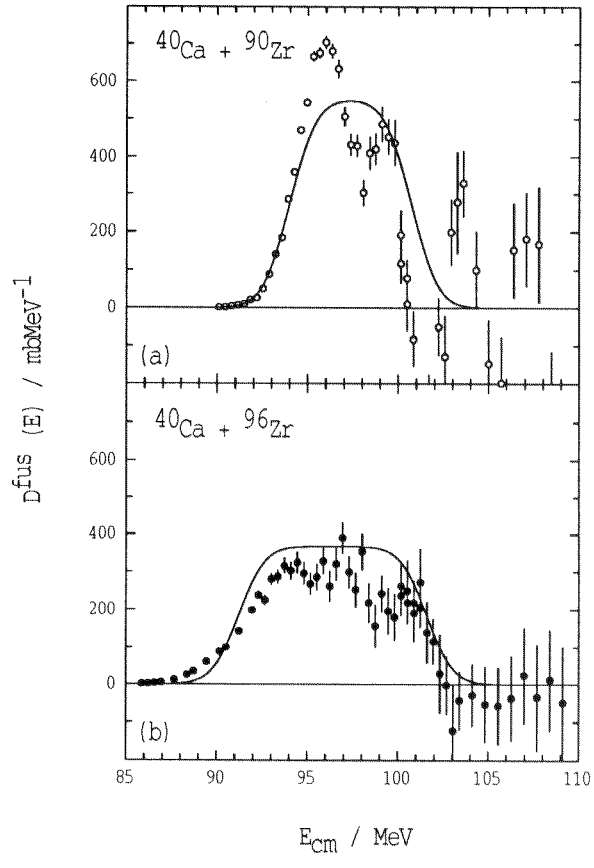

Figure 5.4: *The representations $D^{fus}(E)$ of the barrier distribution for (a) $^{40}Ca + ^{90}Zr$ and (b) $^{40}Ca + ^{96}Zr$. They are compared with the parametrisations of the barrier distribution suggested by the neutron-flow model.*

in the calculations by considering coupling to the lowest energy 2^+ and 3^- states of ^{40}Ca as given in Table 5.1.

The two zirconium isotopes show spherical stability which results partly from the full occupancy of the $Z = 40$ subshells. In ^{90}Zr this stability is additionally enforced by the closure of the $N = 50$ shell, whereas in ^{96}Zr the filled $2d_{5/2}$ neutron subshell has an equivalent effect. This makes ^{96}Zr the even-even zirconium isotope which is most similar to the neutron magic ^{90}Zr. Consequently, with respect to their internal structures, the two isotopes should behave similarly in the fusion with ^{40}Ca.

The lowest excited states of ^{90}Zr and ^{96}Zr have $J^\pi = 0_2^+$ and arise[12] from the excitation of a proton pair from the $2p_{1/2}$ to the $1g_{9/2}$ orbital across $Z = 40$. While the excitation energies of these states are low, their reduced matrix elements for

[12]K. Heyde, E.D. Kirchuk, P. Federman, Phys. Rev. C **38** (1988) 984.

Nucleus	E_x	λ^π	$B(E\lambda)$	β_λ
^{40}Ca	3.904	2^+	2.2	0.12
	3.737	3^-	30.7	0.43
^{90}Zr	2.186	2^+	5.2	0.09
	2.319	5^-	9.8	0.12
	2.748	3^-	32.1	0.22
^{96}Zr	1.751	2^+	4.3	0.08
	1.897	3^-	48.0	0.27

Table 5.1: *Excitation energies E_x, angular momenta λ, parities π, reduced matrix elements $B(E\lambda)$ and deformation parameters β_λ of the states which have been included in the simplified coupled-channels calculations. The energies are given in MeV and the reduced matrix elements are in Weisskopf units. [The data are from: Table of Isotopes 7th edition, ed. C.M. Lederer, V.S. Shirley (1978); L.P. Ekström, J. Lyttkens-Linden, Nucl. Dat. Sheets 67 (1992) 579; L.K. Peker, Nucl. Dat. Sheets 68 (1993) 165; S. Raman et al., At. Dat. Nucl. Dat. Tables 36 (1987) 1; R.H. Spear, At. Dat. Nucl. Dat. Tables 42 (1987) 55.]*

decay to the ground-state are, however, considerably smaller than a Weisskopf single particle unit. The lowest energy 2^+ and 3^- states which are listed in Table 5.1 are moderately collective. Thus, compared to these states the excited 0_2^+ states should have a negligible effect on fusion. As shown in Table 5.1, the lowest 2^+ and 3^- states in ^{90,96}Zr have reduced matrix elements of many Weisskopf units and can be expected to couple strongly to the ground state. In both nuclei the strength of the lowest octupole state is considerably larger than the strength of the lowest quadrupole state. All remaining states, with the exception of the 5^- state in ^{90}Zr, decay either primarily to the lowest 0_2^+, 2^+ or 3^- levels or they have small reduced matrix elements and large excitation energies, so that their coupling to the ground state is small.

Some of the levels decaying to the low energy states in ^{96}Zr have been suggested[13] to be possible members of quadrupole-octupole $(2^+,3^-)$ or octupole-octupole $(3^-)^2$ double phonon states. Since double- and multi-phonon excitations have been found to be important in the fusion of other systems[14,15], their effects on the fusion of

[13]G. Molnár *et al.*, Nucl. Phys. A **500** (1989) 43.

[14]A.M. Stefanini *et al.*, Phys. Rev. Lett. **74** (1995) 864.

[15]A.M. Stefanini *et al.*, Phys. Rev. C **52** (1995) R1727.

System	V_0	r_0	a_0	B_0	R_0	$\hbar\omega_0$
^{40}Ca+^{90}Zr	73.143	1.177	0.78	97.36	10.87	3.42
^{40}Ca+^{96}Zr	73.979	1.177	0.78	96.16	11.03	3.38

Table 5.2: *The potential parameters V_0, r_0, a_0, the average barrier heights B_0, the average fusion radii R_0 and the barrier curvatures $\hbar\omega_0$ as they have been used in the simplified coupled-channels calculations. The energies are given in MeV and the lengths are in fm.*

^{40}Ca + ^{90,96}Zr have been studied particularly carefully in these calculations.

5.5.2 Simplified Coupled-Channels Calculations

Using the code CCMOD[16] simplified coupled-channels calculations have been carried out for both systems. This code is a modified version of CCDEF[17,18], with the matrix diagonalization being performed exactly at each value of the inter-nuclear separation r. These calculations employed the potential parameters given in Table 5.2. The potential depth V_0 and the radius parameter r_0 have been obtained from the global Akyüz-Winther potential[19]. The diffuseness parameter suggested by Akyüz and Winther had to be increased to $a_0 = 0.780$ fm to adapt a one-dimensional barrier penetration calculation for ^{40}Ca + ^{90}Zr to the high energy experimental fusion cross sections. This calculation is shown in Figure 5.1(a) as solid curve.

The results of the simplified coupled-channels calculations are presented in the form of $D^{fus}(E)$ in Figures 5.5 and 5.6. As with the data, the differentiation was approximated using the point-difference formula given in Equation 1.60 with $\Delta E_{cm} = 1.75$ MeV. Initially the effects of phonon couplings on the fusion dynamics was studied, whereas the coupling to neutron transfer channels was investigated subsequently.

[16]M. Dasgupta *et al.*, Nucl. Phys. A **539** (1992) 351.

[17]C.H. Dasso, S. Landowne, Comp. Phys. Comm. **46** (1987) 187.

[18]J.O. Fernández Niello, C.H. Dasso, S. Landowne, Comp. Phys. Comm. **54** (1989) 409.

[19]Ö. Akyüz, A. Winther, Proc. Int. School of Physics E. Fermi, ed. R.A. Broglia (1981).

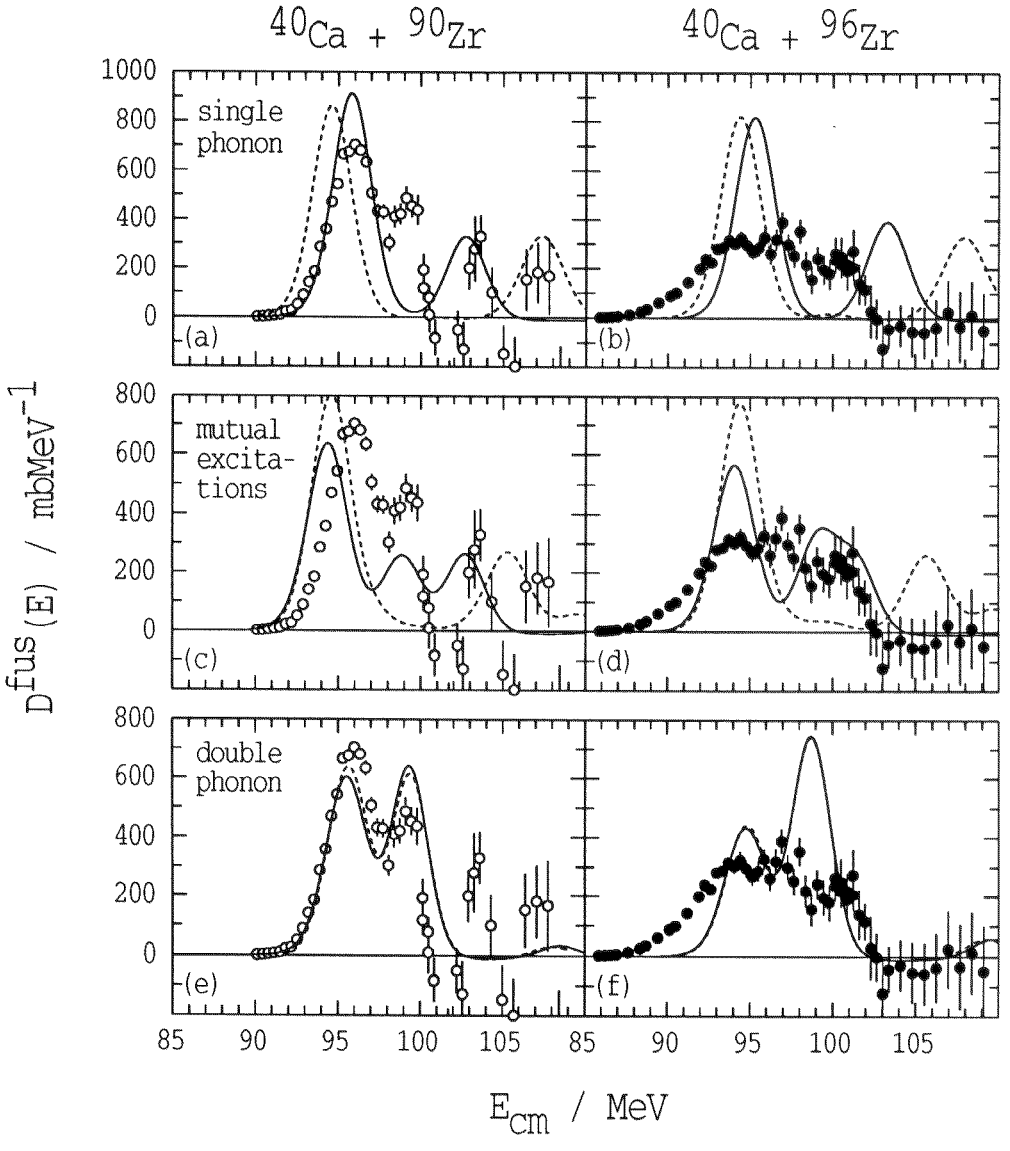

Figure 5.5: *The experimental distributions $D^{fus}(E)$ compared with simplified coupled-channels calculations for phonon coupling. (a,b) Coupling to single phonon excitations. (c,d) Coupling to mutual excitations of projectile and target nucleus. (e,f) Coupling to double phonon excitations of the target nucleus. Details are discussed in the text.*

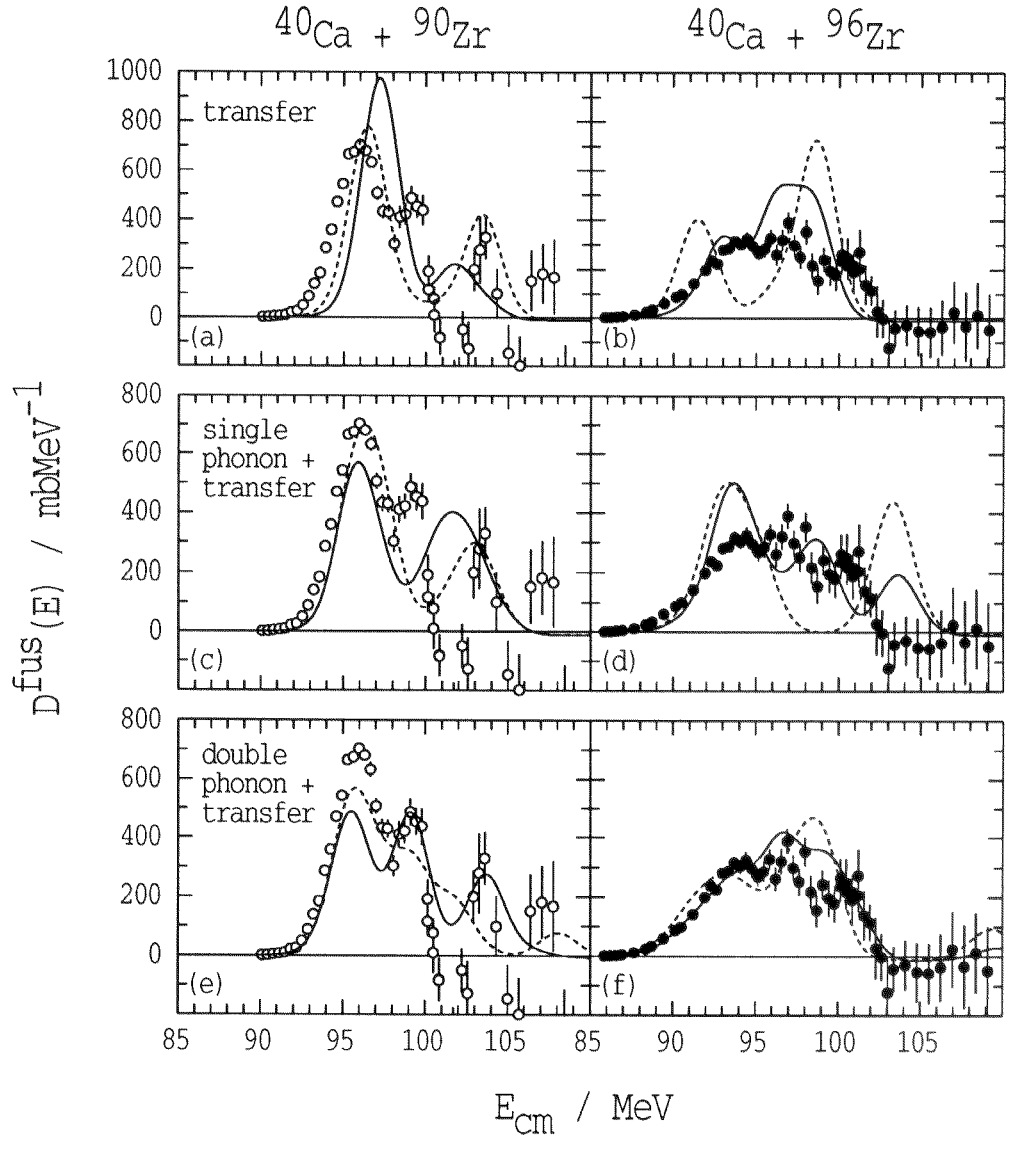

Figure 5.6: *The experimental distributions $D^{fus}(E)$ compared with simplified coupled-channels calculations for coupling to phonons and neutron transfer channels. (a,b) Coupling to neutron transfer only. (c,d) Single phonon coupling combined with neutron transfer. (e,f) Double phonon coupling combined with neutron transfer (e,f). Details are discussed in the text.*

Phonon-Coupling

In CCMOD the coupling strength of a phonon state is estimated from the collective model expression (1.53). The radius of the excited nucleus was chosen as

$$R_a = 1.2\ A^{1/3}\ \text{fm}. \tag{5.1}$$

For ^{40}Ca + ^{90,96}Zr single phonon coupling to the 2^+ and 3^- states of the target nucleus results in the solid curves in Figure 5.5(a,b). For ^{90}Zr this calculation predicts the position of the largest peak correctly. The position of the second peak of the calculation is close to the experimental peak at 103.5 MeV. However, the intermediate peak at 99 MeV is not predicted. For ^{96}Zr there is no agreement between calculation and experiment. For both systems inclusion of the quadrupole state has only a very small effect on the theoretical distribution which is essentially shaped by the coupling to the octupole state. When, in addition to the excitations of the target nucleus, the 2^+ and 3^- states of the projectile are included in the coupling scheme, the separation between the two peaks of the theoretical distribution increases. These calculations are shown as dashed curves in Figure 5.5(a,b) and do not agree with the experimental data.

From the experimental distributions it is obvious that the barrier structures for both systems are more complicated than those calculated with the single phonon coupling scheme. Thus in order to achieve better agreement, this coupling scheme has to be augmented with higher order couplings such as mutual excitations of the reactants or double phonon excitations.

The solid curves in Figure 5.5(c,d) represent calculations which assume single phonon coupling of the 2^+ and 3^- states of the projectile and target nuclei and include in addition couplings to the four mutual excitations $(2_p^+,2_t^+)$, $(2_p^+,3_t^-)$, $(3_p^-,2_t^+)$ and $(3_p^-,3_t^-)$. For ^{40}Ca + ^{90}Zr this coupling scheme approximately reproduces the positions of the three experimental peaks. However, the weights are predicted incorrectly. For ^{40}Ca + ^{96}Zr instead of the two higher peaks the theoretical distribution shows a broad hump. There is no agreement between this calculation and the flat and broad experimental distribution. Omitting the coupling to the $(3_p^-,3_t^-)$ channel results in the dashed curves in Figure 5.5(c,d) which are rather similar to the calculations without mutual excitations in Figure 5.5(a,b). This demonstrates that the double octupole channel is the most important one among the mutual excitations.

From the calculations for ^{40}Ca + ^{90}Zr in Figure 5.5(a,c) it appears that the inclusion of projectile excitations over-predicts the overall coupling strength and

pushes the largest peak down in energy by about 1.5 MeV below its true position. This may be taken as an indication that, in line with the arguments presented before, coupling to projectile excitations is either much reduced or non-existent.

Encouraged by some tentative evidence[20] from spectroscopic studies for double phonon states in ^{96}Zr, further calculations have been carried out for both systems assuming coupling to such excitations in the target nucleus. In these calculations the excitation energies of the unknown double phonon states were assumed to be the sum of the excitation energies of the single phonons involved and the deformation parameters for the double phonon excitations were estimated to be the square root of the quadratic sum of the deformation parameters for the single phonons.

The solid curve in Figure 5.5(e) corresponds to coupling of the 2^+, 3^- single phonon and (2^+,3^-), $(2^+)^2$ and $(3^-)^2$ double phonon states of ^{90}Zr. This calculation is in agreement with the experimental data below $E = 95$ MeV. It predicts the positions of the peaks at $E = 96$ MeV and $E = 99$ MeV correctly and displays also a peak at higher energies which is, however, in a different position than the experimental peak at 103.5 MeV. The dashed curve in Figure 5.5(e) represents a calculation which includes only coupling of the 3^- and $(3^-)^2$ states of ^{90}Zr. It is very similar to the solid curve demonstrating that the two octupole excitations dominate the coupling scheme. The quadrupole couplings modify the calculation only slightly.

The respective calculations for ^{40}Ca + ^{96}Zr are shown in Figure 5.6(f). They are similar to the ones for the lighter system. The calculation which includes only the 3^- and $(3^-)^2$ states of ^{96}Zr is indistinguishable from the one for the complete coupling scheme. In contrast to the lighter system there is no agreement with the experimental data.

The CCMOD calculations which have been presented in the preceding paragraphs exhaust the reasonable coupling schemes involving phonon excitations of up to second order. The inclusion of couplings of even higher order cannot be expected to yield realistic results because of the simplifying approximations which are inherent to the code CCMOD.

For ^{40}Ca + ^{90}Zr the calculations suggest that the coupling scheme of this reaction is dominated by couplings to single and double phonon excitations of the lowest 2^+ and 3^- states in ^{90}Zr, the octupole phonon being strongest. For the heavier system none of the phonon couplings which have been explored predict a barrier

[20] G. Molnár *et al.*, Nucl. Phys. A **500** (1989) 43.

	^{40}Ca + ^{90}Zr		^{40}Ca + ^{96}Zr	
^{40}Ca + xn	simultaneous	sequential	simultaneous	sequential
1n	−3.611	−3.611	+0.509	+0.509
2n	−1.445	+2.166	+5.525	+5.017
3n	−5.861	−4.416	+5.239	−0.287
4n	−4.170	+1.691	+9.637	+4.398
5n	−9.658	−5.488	+8.417	−1.220
6n	−9.038	+0.620	+11.617	+3.200
7n	−14.928	−5.890	+6.919	−4.698
8n	−15.225	−0.297	+7.549	+0.630

Table 5.3: *The Q-values (in MeV) for pick-up of x neutrons by the ^{40}Ca projectile from the target nuclei ^{90}Zr and ^{96}Zr. The values are for simultaneous transfer between the ground states and include the change in the Coulomb barrier energy. The columns labelled 'simultaneous' give the total Q-value, whereas the columns labelled 'sequential' indicate the Q-value for the transfer of the last neutron.*

distribution which displays any similarity with the experimental data. This may be interpreted as an indication that the fusion dynamics of this reaction involves a more complicated coupling scheme.

Coupling to Neutron Transfer

Table 5.3 contains the Q-values for the neutron pick-up reactions

$$^{A}\mathrm{Zr}(^{40}\mathrm{Ca},^{40+x}\mathrm{Ca})^{A-x}\mathrm{Zr} \tag{5.2}$$

For ^{40}Ca + ^{96}Zr up to 8 neutrons can be transferred with positive Q-values from the target to the projectile, whereas for ^{40}Ca + ^{90}Zr the respective Q-values are all negative. This suggests that neutron transfer may play an important role in the fusion of the heavier system. Positive Q-value proton transfer channels also exist in both systems. However, they should be weak, because they involve breaking the $Z = 40$ proton subshell of the zirconium nucleus. In order to explore the effects of neutron transfer on fusion, further CCMOD calculations have been carried out which include coupling to neutron pick-up channels.

In general two schemes of transfer coupling can be distinguished[21-23]. The transfer of neutrons can occur simultaneously or sequentially. Whereas simultaneous transfer occurs in one step, in sequential transfer several nucleons are transferred one after the other, so that the transfer channels are coupled in a chain similar to the states of a rotational band. Such a scheme may be identified with a flow of nucleons.

The effects of transfer are treated only approximately in the code CCMOD using Equation 1.54. In this work the transfer coupling strengths at the position of the one-dimensional barrier and the diffuseness parameter have been chosen to be $F_0 = 4$ MeV and $a_{tr} = 1.2$ fm for all neutron pick-up channels. These values are close to the average values[24]. Transfer to excited states and pairing of the transfer neutrons has been ignored. Consequently, these CCMOD calculations can only be expected to give qualitative results, but they may enable to distinguish qualitatively between the different effects of simultaneous and sequential transfer coupling on the barrier distributions of the two systems.

Figure 5.6(a,b) shows calculations for coupling between the elastic channel and neutron pick-up from the ground state of the target nucleus, while any phonon coupling is neglected. The dashed curves represent coupling to the simultaneous transfer of one, two and three neutrons causing a division of the theoretical distribution into two components. This result was found to be independent from the number of neutrons transferred, as long as the transfer was simultaneous. Additional coupling to single phonon excitations also did not change the double peak structure of the distribution, while only shifting the positions and weights of the peaks. It appears that coupling to simultaneous transfer alone or in combination with single phonon coupling cannot reproduce the complicated barrier structures which are observed for ^{40}Ca + ^{90,96}Zr.

The solid curves in Figure 5.6(a,b) represent calculations which assume the sequential pick-up of 3 neutrons from the ground state, again neglecting phonon couplings. While for ^{40}Ca + ^{90}Zr the calculation displays only two peaks, for ^{40}Ca + ^{96}Zr this coupling scheme results in three peaks which, like the experimental data, merge to form a broad distribution.

The calculations in Figure 5.6(c,d) explore the interplay between single phonon

[21] N. Rowley, Nucl. Phys. A **538** (1992) 205c.

[22] N. Rowley, I.J. Thompson, M.A. Nagarajan, Phys. Lett. B **282** (1992) 276.

[23] A.K. Mohanty, S.K. Kataria, Pramana **43** No. 4 (1994) 319.

[24] G. Pollarolo, R.A. Broglia, A. Winther, Nucl. Phys. A **406** (1983) 369.

and sequential transfer couplings. Single phonon coupling of the lowest 3^- state in the target nucleus and additional sequential coupling of three neutron transfer from the ground state results in the dashed curves which do not agree with the data. The solid curves represent the same coupling scheme, which has, however, been extended to include coupling to the sequential pick-up of two neutrons from the 3^- state. For ^{40}Ca + ^{96}Zr this calculation predicts a distribution consisting of three merged peaks which is not unlike the experimental one, but wider.

The theoretical predictions in Figure 5.6(e,f) assume sequential neutron pick-up in combination with couplings to the 3^- and the $(3^-)^2$ states of the target nucleus. The dashed calculations include sequential transfer of three neutrons from only the ground state. For ^{40}Ca + ^{90}Zr this calculation predicts a triangular shape for the distribution. In the case of ^{40}Ca + ^{96}Zr this coupling scheme produces a theoretical distribution which is qualitatively similar to its experimental counterpart. The solid curves assume the same coupling scheme with additional couplings to the sequential transfer of two neutrons from both the 3^- and the $(3^-)^2$ states. For both systems this results in theoretical distributions which are particularly close to the experimental data. In the case of ^{40}Ca + ^{90}Zr, the three experimental peaks are reproduced, with the exception of the weight of the peak at E_{cm} = 96 MeV which is under-predicts. For ^{40}Ca + ^{96}Zr the theoretical prediction agrees with the experimental data below E_{cm} = 97 MeV and above E_{cm} = 100 MeV.

The simplified coupled-channels calculations which have been presented in the preceding paragraphs suggest that the inclusion of neutron transfer into the coupling scheme can lead to strong modifications of the barrier distribution as it arises from phonon couplings alone. Whereas coupling to simultaneous transfer tends to simply divide the distribution into two components, coupling to sequential transfer can result in complicated barrier structures. It has been found that for the system ^{40}Ca + ^{96}Zr coupling to sequential neutron transfer can cause the broad and flat shape of the experimental distribution. The best agreement with the experimental data for this system is obtained when coupling to single and double phonon excitations of ^{96}Zr is combined with sequential neutron pick-up from the ground state and the excited states. The same coupling scheme gives also the best result for the system ^{40}Ca + ^{90}Zr.

In summary, the simplified coupled-channels calculations suggest a scenario for the fusion of ^{40}Ca + ^{90,96}Zr which involves coupling to single and double phonon excitations of the 2^+ and 3^- states of the target nucleus. In the case of ^{40}Ca + ^{96}Zr additional coupling to sequential neutron pick-up from the ground state and the

excited states is predicted to cause the flattening of the distribution. For ^{40}Ca + ^{90}Zr the extension of the coupling scheme to include neutron pick-up channels may not be necessary to explain the barrier distribution. However, such an extension would still be consistent with the experimental data, as long as the pick-up is sequential and occurs not only from the ground state, but also from excited states.

5.5.3 Exact Coupled-Channels Calculations

Guided by the results of the simplified calculations, exact coupled-channels calculations[25] have been performed for both systems. These calculations included Coulomb excitation, used the iso-centrifugal approximation and an ingoing-wave boundary condition. It was assumed that the nuclear and the Coulomb couplings are equally strong and that the radius of the excited nucleus is given by Equation 5.1. The diffuseness of the nuclear potential was chosen to be $a_0 = 0.9$ fm. The other potential parameters have been obtained by adapting one-dimensional barrier penetration calculations to the high energy cross sections.

The calculations included the 2^+ and 3^- single phonon states of the zirconium target nucleus. The excitation energies and deformation parameters used are given in Table 5.1. For ^{90}Zr the strength of the 5^- state at 2.319 MeV with the deformation parameter $\beta_\lambda = 0.12$ was added in quadrature to the nuclear coupling strength of the quadrupole phonon. In addition to the two single phonon states all three possible double phonon excitations based on the 2^+ and 3^- states were included, namely the $(2^+)^2$, $(3^-)^2$ and $(2^+, 3^-)$ states. Projectile excitation was excluded. The excitation energies and deformation parameters of the double phonon states were the same as in the simplified calculations. The results of the exact coupled-channels calculations are shown in Figure 5.7 and Figure 5.8 where they are compared with the experimental data. The energies have been divided by the average potential barriers B_0 given in Table 5.2.

For ^{40}Ca + ^{90}Zr the calculation reproduces the barrier structure correctly and it agrees with the experimental excitation function. The calculation for ^{40}Ca + ^{96}Zr is similar to the one for the lighter system. Thus it does not predict the barrier structure correctly and under-predicts the excitation function in Figure 5.7 by more than an order of magnitude at the lower energies. Varying the deformation parameters simply shifts the heights and the positions of the peaks in $D^{fus}(E)$. The comparison of the theoretical distributions with the experimental one shows that

[25] N. Rowley, A. Kruppa, *to be published.*

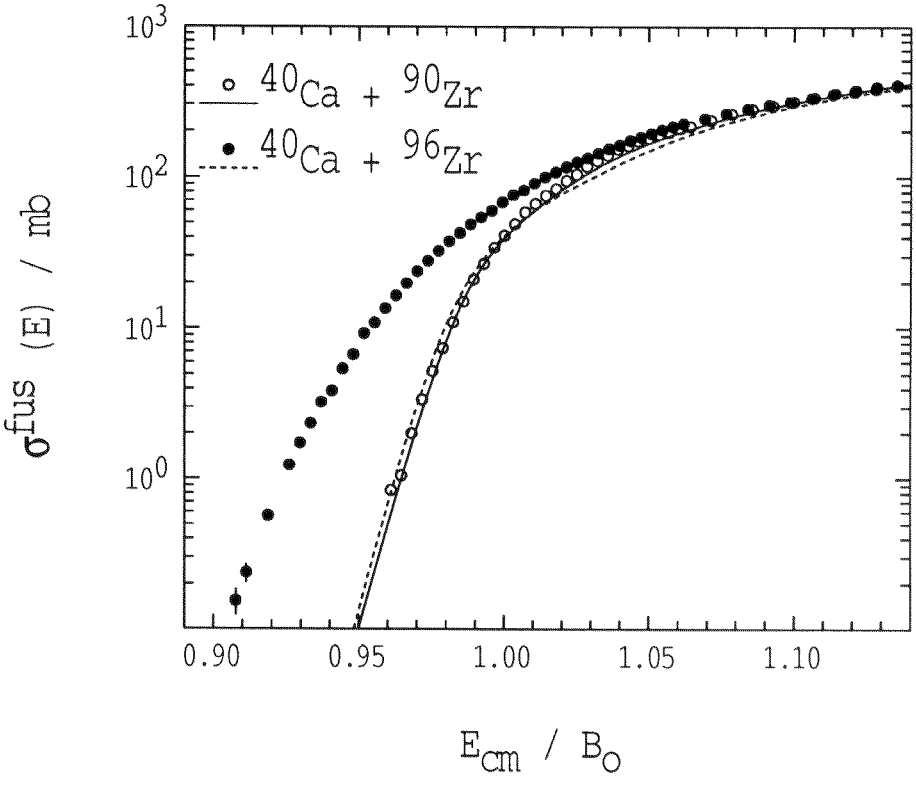

Figure 5.7: *The measured fusion excitation functions compared with exact coupled-channels calculations which assume coupling to single and double phonon excitations of the zirconium nucleus.*

such shifts cannot lead to agreement with the data.

5.6 Concluding Remarks

It can be concluded that the barrier structure and the fusion excitation function for the reaction ^{40}Ca + ^{90}Zr can be explained in terms of the coupling between the relative motion and single and double phonon excitations of ^{90}Zr. In contrast, these couplings are not sufficient to explain the fusion dynamics of the system ^{40}Ca + ^{96}Zr. The similarity of the two zirconium isotopes excludes additional couplings to excited states. Thus the barrier distribution for the heavier system must be affected by neutron transfer, which constitutes the only distinctive difference between the two reactions. It is favoured for ^{96}Zr and unfavoured for ^{90}Zr. The extra six neutrons in ^{96}Zr are outside the $N = 50$ shell, whereas the neutrons in ^{90}Zr are essentially frozen in the full $N = 50$ shell. As a consequence the six 'valence' neutrons in ^{96}Zr

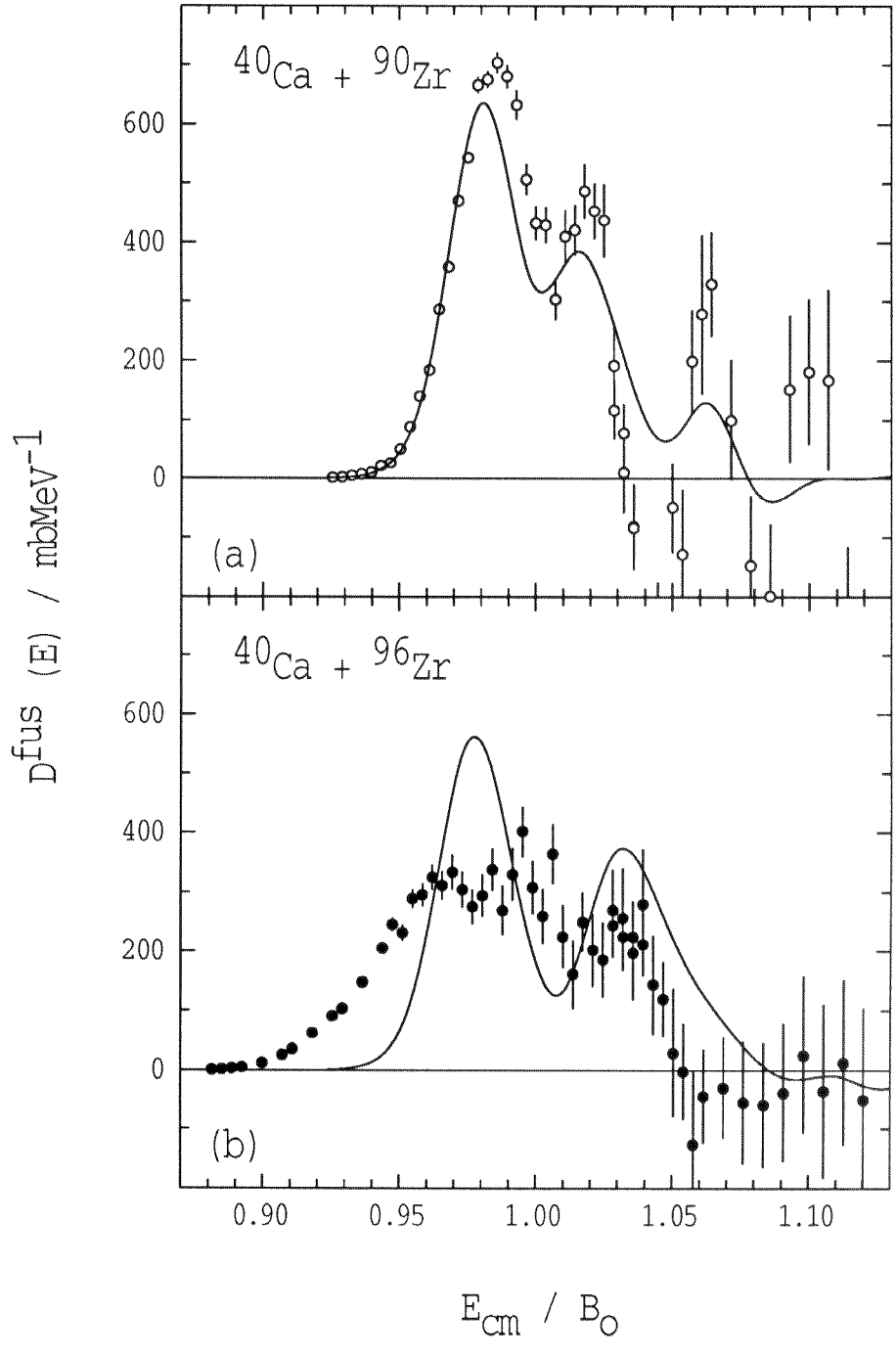

Figure 5.8: *The experimental distributions $D^{fus}(E)$ are compared with exact coupled-channels calculations, which assume coupling to single and double phonon excitations of the zirconium nucleus.*

are more easily transferred to the empty shell outside $N = 20$ in ^{40}Ca.

Simplified coupled-channels calculations suggest that in ^{40}Ca + ^{96}Zr several neutrons may be transferred sequentially. This may be thought of as neutron-flow and interpreted as a precursor of neck-formation. Thus the system ^{40}Ca + ^{96}Zr is a good candidate for a test of the complementarity of the 'microscopic' coupled-channels model and 'macroscopic' transport theories. Such a test, if it is expected to go beyond the results presented here, will require exact coupled-channels calculations, which treat transfer channels in an accurate manner. At the moment the available models of transfer coupling do not match the high quality of the experimental data.